

Evaporation of sessile droplets laden with particles and insoluble surfactants

George Karapetsas,^{*,†} Kirti Chandra Sahu,[‡] and Omar K. Matar[¶]

Department of Chemical Engineering, University of Patras, Patras 26500, Greece,

Department of Chemical Engineering, Indian Institute of Technology Hyderabad,

Sangareddy 502 285, Telangana, India, and Department of Chemical Engineering, Imperial

College London, London SW7 2AZ, UK

E-mail: gkarapetsas@gmail.com

Abstract

We consider the flow dynamics of a thin evaporating droplet in the presence of an insoluble surfactant and non-interacting particles in the bulk. Based on lubrication theory, we derive a set of evolution equations for the film height, the interfacial surfactant and bulk particle concentrations, taking into account the dependence of the liquid viscosity on the local particle concentration. An important ingredient of our model is that it takes into account the fact that the surfactant adsorbed at the interface hinders evaporation. We perform a parametric study to investigate how the presence of surfactants affects the evaporation process as well as the flow dynamics with and without the presence of particles in the bulk. Our numerical calculations show that the droplet life-time is affected significantly by the balance between the ability of surfactant to

*To whom correspondence should be addressed

[†]Department of Chemical Engineering, University of Patras, Patras 26500, Greece

[‡]Department of Chemical Engineering, Indian Institute of Technology Hyderabad, Sangareddy 502 285, Telangana, India

[¶]Department of Chemical Engineering, Imperial College London, London SW7 2AZ, UK

enhance spreading suppressing the effect of thermal Marangoni stresses-induced motion and to hinder the evaporation flux through the reduction of effective interfacial area of evaporation, which tend to accelerate and decelerate the evaporation process, respectively. For particle-laden droplets and in the case of dilute solutions, the droplet life-time is found to be weakly-dependent on the initial particle concentration. We also show that the particle deposition patterns are influenced strongly by the direct effect of surfactant on the evaporative flux; in certain cases, the "coffee stain" effect is enhanced significantly. A discussion of the delicate interplay between the effects of capillary pressure, solutal and thermal Marangoni stresses, which drive the liquid flow inside the evaporating droplet giving rise to the observed results is provided herein.

1. Introduction

Evaporation of droplets containing dispersed particles usually leads to an inhomogeneous residue with the most commonly observed pattern being a thin ring-shaped stain; this phenomenon is widely known as the "coffee stain" or "coffee ring" effect. Besides the pure scientific interest to understand the mechanisms responsible for this effect, it can also be important in a variety of technological applications. Evaporative particle deposition is involved in processes such as the controlled evaporative self-assembly (CESA),¹⁻⁴ fabrication of DNA/RNA micro-arrays,^{5,6} or more traditional ones including for instance printing and coating.

The ability to control the deposition patterns depends strongly on our level of understanding of how the evaporation process takes place and this has led many research groups to undertake experimental and theoretical work in this direction; informative reviews of these efforts can be found in.⁷⁻⁹ The first attempt to shed some light on the "coffee stain" effect came from Deegan et al.¹⁰⁻¹² In these seminal works, it was explained that when the evaporation takes place with a pinned contact line, the ring is produced due to the radial capillary flow from the interior of the drop to the contact line to replenish the liquid that is lost by

evaporation. As a result the particles are carried towards the contact line and are being deposited there. However, as was noted later by Hu and Larson,¹³⁻¹⁵ this is only part of the story since the presence of thermal Marangoni flow may significantly alter the flow field inside the droplet. In particular, it has been shown that in the absence of surfactants, the presence of thermal gradients gives rise to a strong recirculating flow in the droplet leading to particle deposition at the droplet center rather than the edge.¹⁵

Another factor that may affect the flow field is also the presence of any surfactants. In fact, the most common strategy in the literature to control the flow pattern inside an evaporating droplet is to utilize surface active additives in order to induce Marangoni flows; other methods have also been suggested, e.g. the use of electric fields.¹⁶⁻¹⁹ Nevertheless, the mechanisms through which surfactants affect the evaporation process are not well understood and have been a topic of debate. It has been suggested that surfactants can be responsible for suppressing the effect of thermal Marangoni flow by generating a counter gradient of surface tension driving liquid outwards.^{15,20} According to Hu and Larson,¹⁵ given the well known difficulty to keep water surfaces clear of contaminants, this could provide an explanation why in the case of evaporating water droplets the net Marangoni flow was found to be rather weak.¹⁰⁻¹²

Recent experimental studies have shown that depending on the surfactant concentration or the type of surfactant, it is possible to either enhance the "coffee stain" effect or lead to a total flow inversion.²¹⁻²⁷ More specifically, Still et al.²² achieved a uniform deposition of colloidal particles on glass by adding Sodium dodecyl sulfate (SDS) to the drop dispersion. Sempels et al.²⁴ studied a bacterial system, i.e. droplets of cultured *Pseudomonas aeruginosa*, and showed that the auto-production of surfactants suppresses the formation of a coffee ring. However, Crivoi and Duan^{25,26} have shown that the formation of coffee ring of graphite nanoparticles is enhanced with the addition of Cetyltrimethyl Ammonium Bromide (CTAB) surfactant. These authors underlined that the effect of surfactant on the particle sticking probability can also be a decisive factor on the particle deposition pattern. Surfactants also

affect the attachment strength of colloid particles to the solid substrate thus influencing particle deposition.²⁸ Very recently, Anyfantakis et al.²⁹ examined the surfactant mediated interactions between particles and the liquid-gas and liquid-solid interfaces and found that these can also affect the final deposit pattern. The effect of electrostatic and van der Waals forces on the particle deposition process has been examined by Bhardwaj et al.³⁰ Finally, the coexistence of thermal and surfactant concentration gradients may give rise to fingering instabilities at the contact line resulting to depositions with flower like patterns.³¹

To summarize, so far, it has been suggested that the presence of surfactants controls the following effects and phenomena: (a) Marangoni flow due to the presence of interfacial concentration gradients; (b) dynamics of the contact line; (c) particle-particle interactions; (d) particle interactions with liquid-gas and liquid-solid interfaces. It is important to note though, that besides these effects there is also another property of surfactants that has been largely ignored in the study of drying droplets. It is well known in the physical chemistry literature that surfactants may also inhibit the evaporation rate, by reducing the effective area along the liquid-air interface through which evaporation is possible.³²⁻³⁷ One question that arises is how this effect of surfactants on the evaporation flux may affect the flow dynamics and therefore the resulting particle deposition patterns.

The complexity and richness of dynamics due to the presence of coupled heat, mass and momentum transfer phenomena render the study of such systems quite challenging and, as was noted above, most studies so far have relied on experimental observations. In terms of theoretical modelling, people have either considered the case of non-volatile droplets in the presence of surfactants³⁸⁻⁴¹ or evaporating droplets with particles and no surfactants.^{42,43} The scope of this work is to investigate theoretically the case of a thin volatile droplet that contains an insoluble surfactant and non-interacting particles in the bulk.

To this end, we develop a lubrication model based on the so called one-sided approximation⁴⁴⁻⁴⁶ (assuming negligible vapor density, viscosity, and thermal conductivity) which allows us to concentrate solely on the liquid phase. Of course it is anticipated that this

approximation would not be able to provide quantitative predictions in cases where the evaporative process is diffusion limited, and so the vapor phase is relevant. Nevertheless, this approach has proven quite useful in the qualitative description of various phenomena, e.g. the prediction of the emergence of hydrothermal waves in evaporating droplets.⁴⁷ When quantitative predictions are needed the two-sided approach proposed by Sultan et al.⁴⁸ can be more relevant, at the expense of increased complexity of the model. To account for the presence of particles, we employ a simple model applicable to dilute solutions, that has been developed by Warner et al.⁴⁹ for studying evaporating films containing nanoparticles. Finally, we fully account for the presence of insoluble surfactant monomers at the liquid-gas interface. Crucially, our model takes into account the inhibiting effect of the monomers on the evaporative flux which has been ignored by previous works in the literature and thus it is possible to investigate how the droplet dynamics and resulting flow field can be affected by the balance between the ability of surfactant to enhance spreading and to hinder the evaporation flux through the reduction of effective interfacial area of evaporation.

The remainder of the paper is organized as follows. In Section 2, we describe the system of governing equations and outline the numerical scheme that is used for the simulations. The results are presented and discussed in Section 3. Finally, concluding remarks are given in Section 4.

2. Problem formulation

We study the behavior of a droplet undergoing evaporation. The drop is laden with small particles and with an insoluble, non-volatile surfactant which adsorbs at the liquid-air interface. The fluid is considered to be Newtonian, with constant density ρ , specific heat capacity C_p , thermal conductivity λ , and viscosity, μ , which depends on particle concentration. The surface tension, σ , depends on the interfacial concentration of surfactant, Γ , and local temperature, T ; the particles are assumed to be surface-inactive. The drop is placed

on a horizontal solid substrate and bounded from above by an inviscid gas (see Fig. 1). We assume that, initially, the drop has maximal thickness H and half-width L . In the present work, we consider the drop to be very thin and therefore L is assumed to greatly exceed H so that the drop aspect ratio, $\epsilon = H/L$, is assumed to be very small. The latter assumption permits the use of lubrication theory, which will be employed below to derive a set of evolution equations that govern the spreading process.

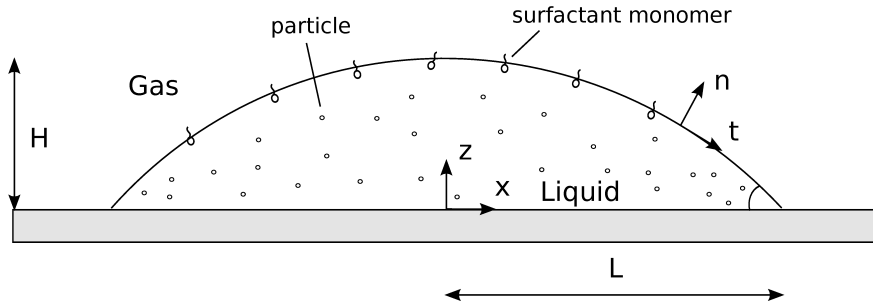


Figure 1: Schematic representation of an evaporating droplet resting on a solid surface of temperature T_w .

We use a Cartesian coordinate system, (x, z) , to model the dynamics and the velocity field, $\mathbf{u} = (u, w)$ where u and w correspond to the horizontal and vertical components of the velocity field, respectively. The liquid-gas interface is located at $z = h(x, t)$ whereas the liquid-solid and the solid-gas interfaces are located at $z = 0$.

The flow is incompressible and governed by the momentum, mass and energy conservation equations, given below:

$$\rho(\mathbf{u}_t + \mathbf{u} \cdot \nabla \mathbf{u}) = \nabla \cdot \boldsymbol{\tau}, \quad (1)$$

$$\nabla \cdot \mathbf{u} = 0, \quad (2)$$

$$\rho C_p (T_t + \mathbf{u} \cdot \nabla T) = \lambda \nabla^2 T, \quad (3)$$

where $\boldsymbol{\tau}$ is the total stress tensor,

$$\boldsymbol{\tau} = -p\mathbf{I} + \mu (\nabla \mathbf{u} + \nabla \mathbf{u}^T), \quad (4)$$

p is the pressure and T is the temperature; ∇ and I denote the gradient operator and identity tensor, respectively. Unless stated otherwise, the subscripts denote partial differentiation with respect to x , z and time t .

Along the free surface ($z = h(x, t)$), it is necessary to distinguish between the liquid velocity, \mathbf{u} and the velocity of the interface $\mathbf{u}_s = (u_s, w_s)$. If J denotes the evaporative flux and $\mathbf{n} = (-h_x, 1)/(1 + h_x^2)^{1/2}$ is the outward unit normal on the interface then

$$\mathbf{u} = \mathbf{u}_s + J/\rho \mathbf{n}, \quad (5)$$

whilst the tangential components of both velocities, $\mathbf{u}_\tau = \mathbf{u} - (\mathbf{u} \cdot \mathbf{n})\mathbf{n} = \mathbf{u}_s - (\mathbf{u}_s \cdot \mathbf{n})\mathbf{n}$, are the same. Moreover, at $z = h(x, t)$ the velocity field satisfies the local mass, force and energy balance in the liquid and gas phase:^{42,47}

$$\rho(\mathbf{u} - \mathbf{u}_s) \cdot \mathbf{n} = \rho_g(\mathbf{u}_g - \mathbf{u}_s) \cdot \mathbf{n}, \quad (6)$$

$$J(\mathbf{u} - \mathbf{u}_g) \cdot \mathbf{n} - \mathbf{n} \cdot (\boldsymbol{\tau} - \boldsymbol{\tau}_g) \cdot \mathbf{n} = 2\kappa\sigma - \Pi, \quad (7)$$

$$J(\mathbf{u} - \mathbf{u}_g) \cdot \mathbf{t} - \mathbf{n} \cdot (\boldsymbol{\tau} - \boldsymbol{\tau}_g) \cdot \mathbf{t} = -\nabla_s \sigma \cdot \mathbf{t}, \quad (8)$$

$$J(L_v + \frac{1}{2}((\mathbf{u}_g - \mathbf{u}_s) \cdot \mathbf{n})^2 - \frac{1}{2}((\mathbf{u} - \mathbf{u}_s) \cdot \mathbf{n})^2) + \lambda \nabla T \cdot \mathbf{n} - \lambda_g \nabla T_g \cdot \mathbf{n} + \quad (9)$$

$$(\boldsymbol{\tau} \cdot \mathbf{n}) \cdot (\mathbf{u} - \mathbf{u}_s) - (\boldsymbol{\tau}_g \cdot \mathbf{n}) \cdot (\mathbf{u}_g - \mathbf{u}_s) = 0.$$

Here ρ_g , λ_g , \mathbf{u}_g , T_g , denote the density, thermal conductivity, velocity field and temperature in the gas phase, respectively; L_v is the specific internal latent heat of vaporization.⁵⁰ $\mathbf{t} = (1, h_x)/(1 + h_x^2)^{1/2}$ denotes the unit tangential vectors on the interface. 2κ is the mean curvature of the free surface and ∇_s is the surface gradient operator, respectively defined as

$$2\kappa = \nabla_s \cdot \mathbf{n}, \quad \nabla_s = (I - \mathbf{nn}) \cdot \nabla. \quad (10)$$

Π denotes the disjoining pressure, which accounts for the van der Waals interactions, defined

as

$$\Pi = \frac{A}{6\pi h^3}, \quad (11)$$

where A is the Hamaker constant.

Along the moving interface ($z = h(x, t)$) we also impose the kinematic boundary condition,

$$h_t + u_s h_x = w_s. \quad (12)$$

At the liquid-solid interface ($z = 0$), we set

$$u = 0, \quad w = 0, \quad T = T_w. \quad (13)$$

Surfactant and particle transport

We consider that the droplet contains small particles with an initially uniform concentration, c_i . The concentration of particles in the bulk, c , is governed by an advection-diffusion equation

$$c_t + \mathbf{u} \cdot \nabla c = D_c \nabla^2 c, \quad (14)$$

subject to the following boundary conditions

$$(\mathbf{n} \cdot \nabla c)_{z=0} = 0, \quad (15)$$

$$D_c (\mathbf{n} \cdot \nabla c)_{z=h} = c (\mathbf{u} - \mathbf{u}_s) \cdot \mathbf{n}. \quad (16)$$

The viscosity of the fluid, $\mu(c)$, is assumed to be dependent locally on the concentration of particles in the bulk, c , through the following constitutive relation:^{51,52}

$$\mu(c) = \mu_c \left(1 - \frac{c}{c_\infty}\right)^{-2}. \quad (17)$$

Here, c_∞ represents the maximum packing of the bulk particles; the magnitude of this parameter is determined by factors such as particle size, shape, and packing configuration. A restriction of the present model is that it is applicable to dilute solutions. It should be noted though that as the droplet dries out the concentration of particles will increase and eventually become so high that this assumption will no longer hold. To properly account for this transition a more complex model would be needed, e.g. see Kaplan & Mahadevan.^{43,53}

The behaviour of the surfactant monomers is modelled by the following advection-diffusion equation:

$$\Gamma_t - h_t(\mathbf{e}_z \cdot \nabla_s \Gamma) + \nabla_s \cdot (\mathbf{u}_\tau \Gamma) + (\nabla_s \cdot \mathbf{n})(\mathbf{u}_s \cdot \mathbf{n})\Gamma = D_\Gamma \nabla_s^2 \Gamma, \quad (18)$$

where D_Γ denotes the diffusion coefficient of the monomers at the liquid-air interface. As explained in Refs.^{37,54,55} the first two terms on the left hand side together describe the temporal change of Γ along the normal to the moving interface, the third term accounts for the advection of the surfactant due to the liquid flow along the interface and the fourth term accounts for the variation in surfactant concentration resulting from local changes in interfacial area. Note that the total mass of the surfactant, M_{surf} , and particles, M_{par} , present in the liquid drop are conserved quantities, given by

$$\begin{aligned} \int_0^L \Gamma dx &= M_{surf}, \\ \int_0^L \int_0^h c dz dx &= M_{par}. \end{aligned} \quad (19)$$

Constitutive equations for surface tension and evaporative flux

To complete the description, a constitutive equation that describes the dependence of the interfacial tension on the surfactant concentration and interfacial temperature is required.

To this end, we employ the following constitutive equation

$$\sigma = \sigma_c \left(1 + \frac{\Gamma}{\Gamma_\infty} \left[\left(\frac{\sigma_c}{\sigma_m} \right)^{1/3} - 1 \right] \right)^{-3} + \frac{\partial \sigma}{\partial T} \Big|_{\Gamma=0} (T - T_{sat}), \quad (20)$$

which is based on the Sheludko equation of state^{56,57} and assumes a linear dependence on the temperature. Here, σ_c and σ_m are the surface tensions at $T = T_{sat}$ of a surfactant-free fluid and of maximal surfactant concentration, respectively.

Finally, we use the following non-equilibrium interfacial condition to model evaporative effects^{45,46,58}

$$\frac{p_{ve}}{p_v} - 1 = \frac{p - p_v}{\rho R_g T_{sat}} + \frac{L_v}{R_g T_{sat}} \left(\frac{T|_h}{T_{sat}} - 1 \right), \quad (21)$$

where p_{ve} is the equilibrium vapour pressure, $T|_h$ is the interfacial temperature and R_g denotes the specific gas constant. **The following equilibrium relation is also used for the evaporative flux, J ⁵⁸**

$$J = \rho_v \left(\frac{R_g T_{sat}}{2\pi} \right)^{1/2} \left(\alpha_v \frac{p_{ve}}{p_v} - \beta_v \right). \quad (22)$$

In this expression α_v and β_v are accommodation coefficients for evaporation and condensation, respectively. Near equilibrium, we note that α_v and β_v will be nearly equal. The surfactant adsorbed at the surface hinders the evaporation and to account for this effect we assume the following dependence on the interfacial surfactant concentration

$$\alpha_v(\Gamma) = \beta_v(\Gamma) = \frac{\Gamma_\infty}{\Gamma_\infty + \psi\Gamma}, \quad (23)$$

where $\psi > 0$. At maximum packing the accommodation coefficient becomes equal to $1/(1 + \psi)$ and this limit may be used for an estimation of ψ from experimental data. A typical range for the accommodation coefficients is between 0.001 to 1 which implies that $0 < \psi < 10^3$. In what follows, the effect of ψ on the evaporation will be studied.

Scaling

The governing equations and boundary conditions are made dimensionless using the following scalings (tildes denote dimensionless variables):

$$\begin{aligned}
(x, z, h) &= L(\tilde{x}, \epsilon\tilde{z}, \epsilon\tilde{h}), \quad t = \frac{L}{U}\tilde{t}, \quad (u, w) = U(\tilde{u}, \epsilon\tilde{w}), \\
(p, \Pi) &= \frac{\mu_c UL}{H^2}(\tilde{p}, \tilde{\Pi}), \quad T = \tilde{T}(T_w - T_{sat}) + T_{sat}, \quad \sigma = \tilde{\sigma}\sigma_c, \\
J &= \tilde{J}\frac{\lambda(T_w - T_{sat})}{HL_v}, \quad \Gamma = \tilde{\Gamma}\Gamma_\infty, \quad c = \tilde{c}c_i, \\
M_{surf} &= \tilde{M}_{surf}L\Gamma_\infty, \quad M_{par} = \tilde{M}_{par}LHc_i,
\end{aligned} \tag{24}$$

where $U = \epsilon\sigma_c/\mu_c$ is a characteristic velocity. The tildes are henceforth suppressed. Substitution of these scalings into the governing equations and boundary conditions, using the lubrication approximation ($\epsilon \ll 1$), yields

$$u_x + w_z = 0, \tag{25}$$

$$p_x = (\mu u_z)_z, \quad p_z = 0, \tag{26}$$

$$T_{zz} = 0, \tag{27}$$

$$c_t + uc_x + wc_z = \frac{1}{Pe_c} \left(c_{xx} + \frac{c_{zz}}{\epsilon^2} \right), \tag{28}$$

and

$$\Gamma_t + (u\Gamma)_x = \frac{\Gamma_{xx}}{Pe_\Gamma} \quad \text{at } z = h. \tag{29}$$

The dimensionless viscosity is given by

$$\mu = (1 - \chi c)^{-2}, \tag{30}$$

where $\chi = c_i/c_\infty$. The dimensionless groups $Pe_i = UL/D_i$ ($i = \Gamma, c$) are Peclet numbers representing a ratio of convective to diffusive time scales for the monomers at the free surface, and the particles in the bulk, respectively.

Solution of the above equations are obtained subject to the following boundary conditions at the solid wall ($z = 0$)

$$u = 0, \quad w = 0, \quad T = 1. \tag{31}$$

Along the liquid-gas interface, $z = h(x, t)$, the boundary conditions become

$$\begin{aligned}
h_t + uh_x - w + EJ &= 0, \\
u_z &= \frac{\sigma_x}{\mu}, \\
p &= p_v + \mathcal{R}J^2 - \epsilon^2 \sigma h_{xx} - \frac{\mathcal{A}}{h^3}, \\
J \left(1 + \frac{E^2}{2\mathcal{L}D} J^2 \right) + T_z &= 0,
\end{aligned} \tag{32}$$

where $E = \lambda(T_w - T_{sat})/(\epsilon U \rho H L_v)$ is the evaporation number, $\mathcal{A} = A/(6\pi H L \mu U)$ is the dimensionless Hamaker constant, $\mathcal{R} = \epsilon \lambda^2 (T_w - T_{sat})^2 / (L_v^2 \rho_g \mu_c U H)$ is the vapor recoil number, $\mathcal{L} = \epsilon^2 L_v / U^2$ and $D = \epsilon^{-2} \rho_g / \rho$. Here we have adopted the one sided-model⁴⁴ assuming that $(\rho_g/\rho, \mu_g/\mu_c, \lambda_g/\lambda) \ll 1$. Typical values of the physical properties are given in Table 1 along with a typical range of all the dimensionless parameters. As it is shown in Table 1, the parameters \mathcal{R} and \mathcal{L} are typically small and the model may be further simplified by assuming that $\mathcal{R} \ll 1$ and $\mathcal{K} \ll 1$.

Table 1: Order of magnitude estimates of the physical constants and typical range of the dimensionless parameters

Constants	Typical values	Parameter	Typical range
L (m)	10^{-3}	ϵ	0.005 – 0.2
μ_c (Pas)	10^{-3}	E	0 – 0.001
ρ (kg/m ³)	10^3	K	10^{-5} – 0.1
λ (W/mK)	0.5	D	0.1 – 10^2
μ_g (Pas)	10^{-5}	Σ	1 – 5
ρ_g (kg/m ³)	1	ψ	0 – 10^3
λ_g (W/mK)	0.02	χ	0.01 – 0.1
σ_c (N/m)	0.07	Pe_Γ	10^2 – 10^6
L_v (J/kg)	10^6	Pe_c	10 – 10^5
A (J)	10^{-19}	\mathcal{R}	10^{-4} – 0.1
		\mathcal{L}	1 – 10^3
		\mathcal{A}	10^{-5} – 10^{-9}
		Δ	10^{-3} – 10^{-7}

The constitutive equation for the evaporative flux is given by

$$(1 + \psi\Gamma)KJ = \Delta(p - p_v) + T|_h, \quad (33)$$

where

$$\Delta = \frac{\mu_c U L T_{sat}}{\rho H^2 L_v (T_w - T_{sat})}, \quad K = \frac{\lambda (2\pi R_g T_{sat}^3)^{1/2}}{\rho_g H L_v^2}. \quad (34)$$

By solving Eqs. (25)-(27) subject to boundary conditions (31) and (32), and adopting the rapid vertical diffusion approximation for the bulk concentrations,^{41,59} we can derive the following equations

$$h_t = \left(\frac{h^3}{3\mu} p_x - \sigma_x \frac{h^2}{2\mu} \right)_x - EJ, \quad (35)$$

$$T = 1 - Jz, \quad (36)$$

$$\Gamma_t + (u\Gamma)_x = \frac{\Gamma_{xx}}{Pe_\Gamma}, \quad (37)$$

$$c_t + \bar{u}c_x = \frac{1}{Pe_c} \frac{(hc_x)_x}{h} + \frac{EJc}{h}, \quad (38)$$

where the pressure gradient and average streamwise velocity component are respectively given by

$$p_x = -\epsilon^2 (\sigma h_{xx})_x - \Pi_x, \quad (39)$$

$$\bar{u} = -\frac{h^2}{3\mu} p_x + \sigma_x \frac{h}{2\mu}; \quad (40)$$

we have retained capillary contributions despite the fact that they arise to order $O(\epsilon^2)$ in our model since we expect them to provide non-negligible contributions in highly-curved regions in the flow.⁶⁰ Here, Π denotes the dimensionless disjoining pressure, $\Pi = \mathcal{A}/h^3$. In the above equations, the evaporative flux, J , is evaluated using the following expression

$$J = \frac{-\Delta \left[\epsilon^2 \left([1 + \Gamma (\Sigma^{1/3} - 1)]^{-3} - \gamma \right) h_{xx} + \mathcal{A}/h^3 \right] + 1}{(1 + \psi\Gamma)K + h(\Delta\epsilon^2\gamma h_{xx} + 1)}; \quad (41)$$

the dimensionless form of the equation of state for the liquid-gas surface tension is given by

$$\sigma = [1 + \Gamma (\Sigma^{1/3} - 1)]^{-3} - \gamma T, \quad (42)$$

where $\Sigma = \sigma_c/\sigma_m$ and $\gamma = -\partial\sigma/\partial T|_{\Gamma=0}(T_w - T_{sat})/\sigma_c$. We note that the effect of surfactants on J enters through the parameter ψ (and also through the dependence of σ on Γ in the capillary contribution to the pressure).

It is useful to note that the bulk average velocity, \bar{u} , given by Eq. (40) can be also decomposed as follows

$$\bar{u} = \bar{u}_{ca} + \bar{u}_{cg} + \bar{u}_{tg}, \quad (43)$$

where each contribution is expressed by

$$\bar{u}_{ca} = -\frac{h^2}{3\mu}p_x, \quad \bar{u}_{cg} = -\frac{3\Gamma_x(\Sigma^{1/3} - 1)}{[1 + \Gamma(\Sigma^{1/3} - 1)]^4} \frac{h}{2\mu}, \quad \bar{u}_{tg} = -\gamma T_x \frac{h}{2\mu}. \quad (44)$$

Each of the three different components corresponds to a different mechanism that acts to drive liquid inside the evaporating droplet. Here, \bar{u}_{ca} denotes the velocity that is caused by the presence of the capillary effects, while \bar{u}_{cg} and \bar{u}_{tg} correspond to effect of Marangoni stresses. More specifically, \bar{u}_{cg} denotes the velocity due to the presence of surfactant concentration gradients, while \bar{u}_{tg} denotes the velocity due to the thermal gradients along the interface.

Initial and boundary conditions

Solutions are obtained starting from the following initial conditions for h , T , c and Γ , which correspond to a droplet with constant curvature at rest with uniform temperature and all

species in equilibrium.

$$\begin{aligned}
 h(x, t = 0) &= \max[h_\infty, 1 - x^2], \\
 (\Gamma, c)(x, t = 0) &= 0.5 (1 + \tanh [100(1 - x)]), \\
 T(x, t = 0) &= 1.
 \end{aligned}
 \tag{45}$$

In addition, we assume that the droplet is released onto an ultra thin-film of uniform thickness

$$h_\infty = (\mathcal{A}\Delta)^{1/3}. \tag{46}$$

This film is adsorbed from the atmosphere and it is stabilized by van der Waals forces. The presence of this film, which is stabilized due to the fact that evaporation becomes suppressed by the action of attractive van der Waals forces, helps alleviate the stress singularity that could arise at the moving contact line. Regarding the boundary conditions in the x -direction, we impose the following

$$\begin{aligned}
 h_x(0, t) = h_{xxx}(0, t) = h_x(x_\infty, t) = h_{xxx}(x_\infty, t) &= 0, \\
 (\Gamma_x, c_x)(0, t) = (\Gamma_x, c_x)(x_\infty, t) &= 0.
 \end{aligned}
 \tag{47}$$

3. Results and Discussion

The evaporation of a surfactant-laden liquid drop with particles is a parametrically-rich problem. We begin our study by examining the flow in the case of an insoluble surfactant without particles and proceed with simulations in the presence of a finite particle concentration to examine the effect of various system parameters on the resulting particle deposition. Numerical solutions were obtained over a wide range of parameter values. The ‘base’ case, however, is characterized by parameter values that are broadly typical of experimental settings: $\epsilon = 0.1$, $K = 0.1$, $\Sigma = 5$, $\mathcal{A} = 10^{-6}$, $\Delta = 10^{-3}$, $Pe_\Gamma = 10^3$, $Pe_c = 10$; these values will be kept constant unless otherwise noted. In the parametric study that will be presented

below we will vary the parameters M_{surf} , ψ , γ , E , M_{par} and χ . According to Eq. (46) for the given set of parameters the height of the precursor film used is $h_\infty = 10^{-3}$.

3.1 Surfactant-laden droplets without particles

3.1.1 $\psi = 0$

We begin our study by examining first the evaporation process of a particle-free droplet. For the moment we will not take into account the effect of surfactant on the evaporative flux and neglect the primary dependence of J on Γ by setting $\psi = 0$; we note that J remains dependent on Γ through the capillary pressure term in the numerator of Eq. (41). In Fig. 2(a,b), we show the spatio-temporal variation of the drop height, for the particle-free case, in the presence and absence of surfactant, respectively. In the surfactant-free case, the droplet dewets the surface during all stages of the evaporation process as is evident from Fig. 2(c), which demonstrates that the contact line location, x_c , undergoes a monotonic decrease with time. This decrease is retarded during the intermediate stages of droplet evaporation, which can be attributed to the fact that near the contact line region the capillary flow becomes stronger drawing more liquid towards the contact line in contrast to the surfactant-laden case; this is demonstrated in Fig. 3(a,b) where we plot the profile of \bar{u}_{ca} , i.e. the velocity component which is due to the capillary pressure. The presence of thermal gradients gives rise to thermal Marangoni stresses which drive liquid towards the droplet centre thus leading to the increase of the interfacial height at the droplet apex during an intermediate stage of the dynamics before decreasing monotonically with time; this is also depicted clearly in the inset of Fig. 2(c). An animation of the droplet profile along with the velocity field (x -component) and the streamlines is given in the Supporting Information (Movies S1 and S2). Snapshots at two time instants ($t = 10, 50$) are depicted in Fig. 4 for (a,b,c) $M_{surf} = 0$ (see Movie S1) and (d,e,f) $M_{surf} = 0.5$ (see Movie S2); (c,f) depict a zoom near the contact line at $t = 50$. Here, it is shown clearly that the thermal Marangoni stresses give rise to a recirculation vortex, which grows significantly until it engulfs the whole droplet; the direction of the vortex is in

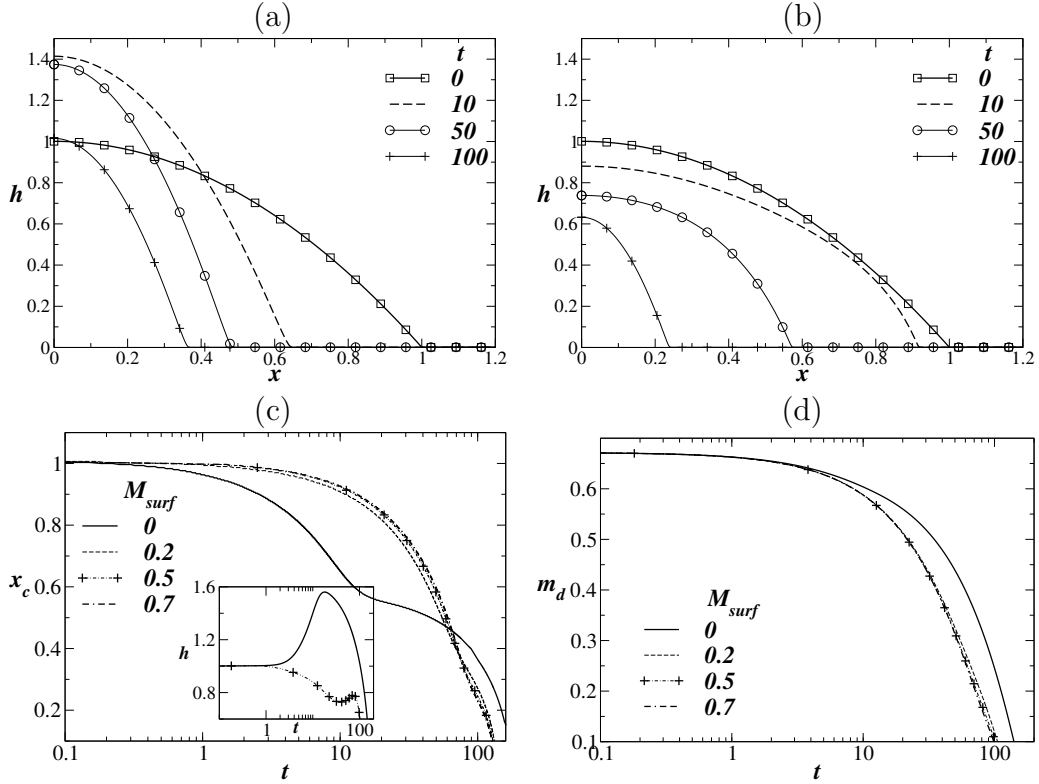


Figure 2: Evolution of the drop profile for (a) $M_{surf} = 0$, and (b) $M_{surf} = 0.5$. Evolution of the (c) position of the contact line and (d) mass of the drop for different values of M_{surf} . The rest of the parameter values are $E = 0.005$, $M_{par} = 0$, $\psi = 0$, $\chi = 0$ and $\gamma = 0.1$. The inset to panel (c) also shows the temporal evolution of the maximal film thickness, h_{max} , for $M_{surf} = 0$ and $M_{surf} = 0.5$ shown by solid and dashed lines, respectively.

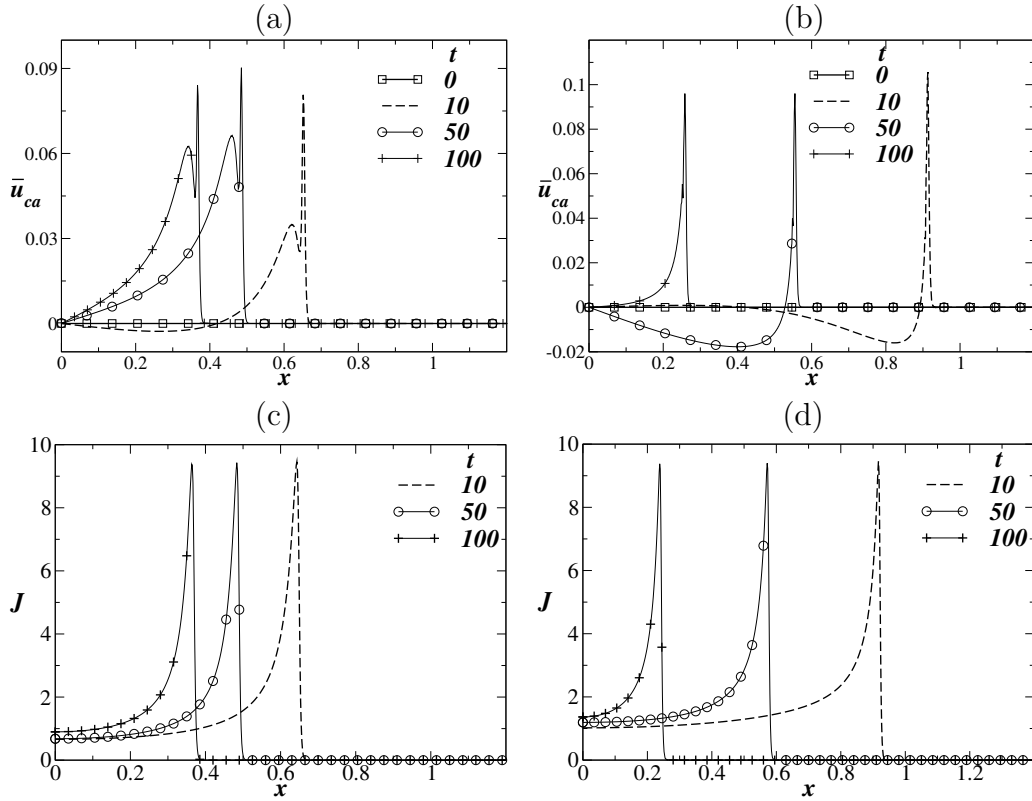


Figure 3: Profiles of \bar{u}_{ca} at different time instants for (a) $M_{surf} = 0$, and (b) $M_{surf} = 0.5$. Profiles of the evaporative flux, J , at different time instants for (c) $M_{surf} = 0$, and (d) $M_{surf} = 0.5$. The rest of the parameter values are $E = 0.005$, $M_{par} = 0$, $\psi = 0$, $\chi = 0$ and $\gamma = 0.1$.

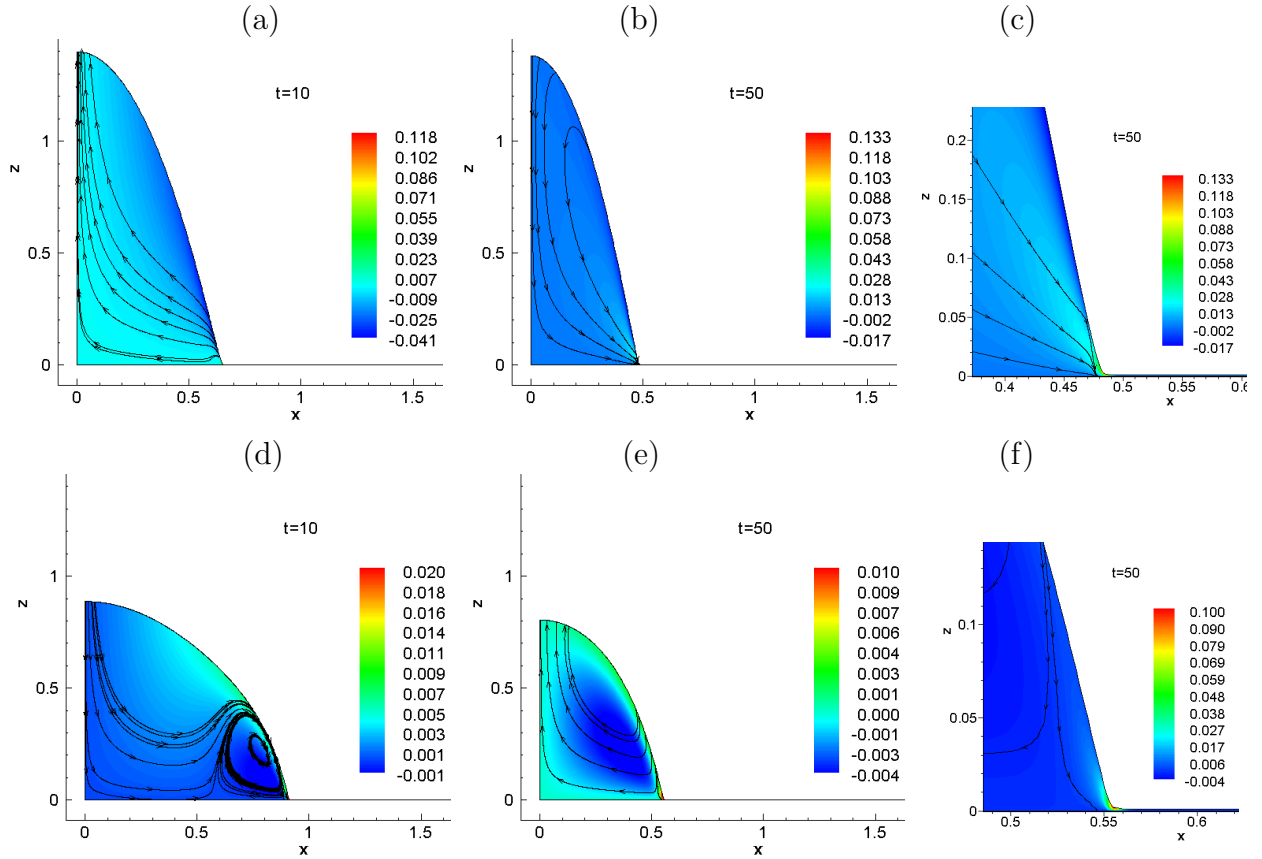


Figure 4: Contour plots of x -velocity, u , along with streamlines for (a,b,c) $M_{surf} = 0$ and (d,e,f) $M_{surf} = 0.5$ at $t = 10, 50$; (c,f) depict a zoom near the contact line at $t = 50$. The rest of the parameter values are $E = 0.005$, $M_{par} = 0$, $\psi = 0$, $\chi = 0$ and $\gamma = 0.1$. Animations of these simulations are available: (a,b,c) Movie S1 and (d,e,f) Movie S2 in Supporting Information.

agreement with previous studies for substrates of infinite conductivity.^{13,15,61} The action of thermal Marangoni stresses is also responsible for the enhancement of the dewetting process.

In the presence of surfactant, the droplet does not retract during the early stages of the evaporation process. In fact, the contact line position remains essentially pinned up to $O(1)$ time-scales before receding. As shown in Fig. 2(b,c), the dewetting process is not accompanied by an increase in the droplet thickness at the flow origin (see inset of Fig. 2(c)), and although there appears to be a retardation of the contact line recession during the latest stages of evaporation, it is much less significant than the surfactant-free case. A more detailed look in the flow field (see Fig. 4(d,e,f)) reveals a drastic change due to the effect of surfactants. At early times a counter rotating vortex arises in the contact line region, which grows and eventually takes over; a stagnation point also arises in the contact line region (see Fig. 4f). These results are in line with experimental observations.^{22,27} As will be shown below, this is merely due to the action of surfactant concentration gradients which significantly reduce or even neutralise the effect of thermal Marangoni stresses. Inspection of the temporal variation of the droplet mass, m_d , shown in Fig. 2(d), also reveals that the presence of surfactant accelerates the evaporation process, though one should note again that the effect of surfactant on the evaporative flux has been largely neglected in generating these results by setting $\psi = 0$ (though the Γ contribution to the capillary pressure in J [see Eq. (41)] remains).

In Fig. 3(c) and 3(d), we show the development of the evaporative flux, J , during the dynamics for the surfactant-free and surfactant-laden cases, and the same parameters used to generate Fig. 2. For the results shown in this figure, for which $\psi = 0$, it appears that the surfactant makes little difference to the overall structure of J and its maximal value. The latter observation is a clear indication that the acceleration of droplet evaporation should actually be attributed to the fact that the droplet remains flatter for longer times which leads to an increase of the effective interfacial area of evaporation. As is depicted in Fig. 3(c,d), the evaporative flux is highly localized in the contact line region, where it can be

approximated by

$$J \sim \frac{1 - \Delta\Pi}{(1 + \psi\Gamma)K}. \quad (48)$$

The flux exhibits a long, decay ‘tail’ towards the droplet apex where its value is given by the following approximate formula:

$$J \sim \frac{1}{h + (1 + \psi\Gamma)K}. \quad (49)$$

In the $\psi = 0$ case, Eqs. (48) and (49) reduce to $J \sim (1 - \Delta\Pi)/K$ and $J \sim 1/(h + K)$, respectively.

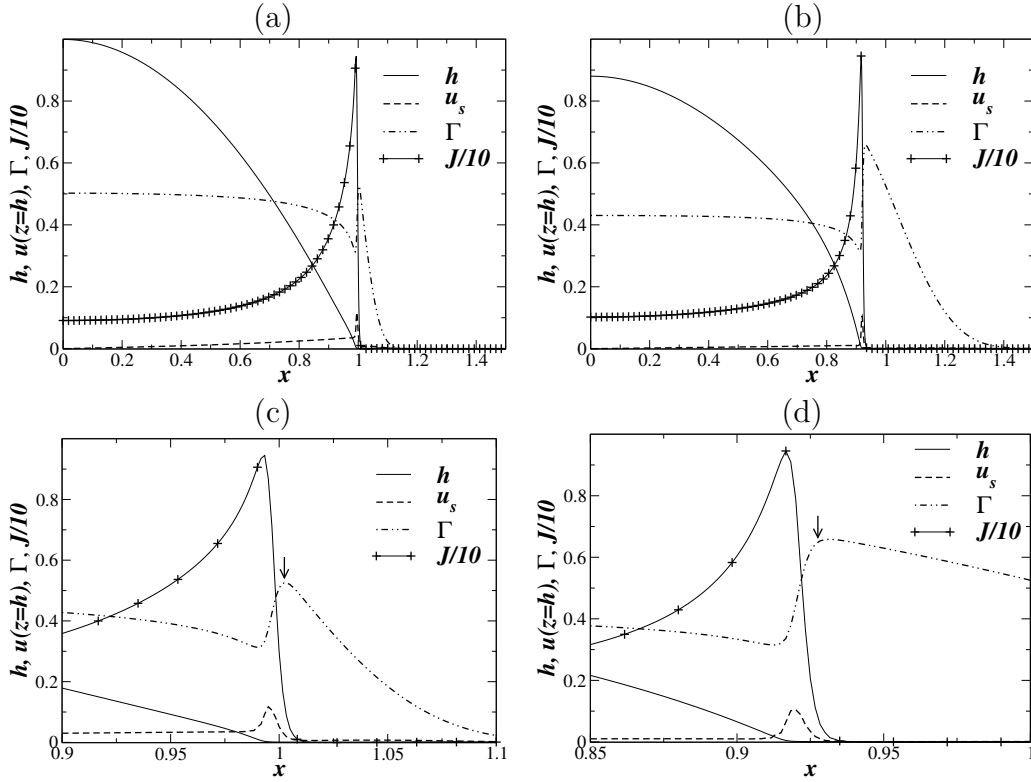


Figure 5: Profiles of the drop height, h , streamwise liquid velocity at the interface, $u(z = h)$, surfactant concentration, Γ , and evaporative flux, J , at (a) $t = 1$ and (b) $t = 10$. The corresponding zoomed views are presented in panels (c) and (d), respectively. The rest of the parameter values are $M_{surf} = 0.5$, $M_{par} = 0$, $\psi = 0$, $\chi = 0$ and $\gamma = 0.1$.

The location of the evaporative flux in relation to the contact line is shown more clearly in Fig. 5 for the surfactant-laden case ($M_{surf} = 0.5$) at $t = 1$ and $t = 10$ during the

dynamics in panels (a) and (b), with enlarged versions of the contact line region depicted in panels (c) and (d), respectively. Also shown in this figure are the corresponding profiles for the interfacial surfactant concentration, Γ , and the streamwise component of the interfacial velocity, $u(z = h)$. It is seen that Γ remains approximately constant over a large proportion of the drop before undergoing a rapid decrease as the contact line region is approached. The concentration Γ then exhibits a sharp increase to a maximal value (indicated by the arrows in panels (c,d)) located immediately downstream of the contact line and the location of the maximal value of J ; this is followed by a decay to zero in the precursor film region. The spatial profile of Γ is reminiscent of the profile seen in the case of surfactant enhanced spreading in the absence of evaporation.⁴¹ A major difference is that here we do not account for the explicit presence of a contact line as was done by⁴¹ but use instead a precursor model to relieve the contact line singularity.

Therefore, in our case the surfactant is allowed to diffuse ahead of the contact line which is responsible for the decay of Γ in that region; note that there is no flow present in the precursor film. Such a behaviour is not unreasonable and would actually be expected in the case of a prewetted solid surface; it could also resemble the case where the surfactant adsorbs at the solid substrate through the contact line and diffuse ahead of the drop.^{41,59} It is also seen in Fig. 4(c) and (d) that the interfacial liquid velocity $u(z = h)$ increases gradually within the drop due to the Marangoni contribution from $h\Gamma_x$, before undergoing rapid variation in the immediate vicinity of the contact line region where it exhibits a maximum due to the strong capillary flow there; beyond its maximal value, $u(z = h)$ decays rapidly to zero in the precursor film.

3.1.2 $\psi > 0$

Next, we examine the effect of surfactant on the evaporation by exploring the influence of the parameter ψ on the temporal evolution of the droplet mass. Inspection of Fig. 6(a) reveals that an increase in ψ has an overall retarding effect on the evaporation process,

leading to an increase in the droplet life-time. This may also be expected by appealing to Eq. (48): it is clear from this expression that increasing ψ leads to a decrease in J , and this is responsible for the trends shown in Fig. 6(a). From this expression we also

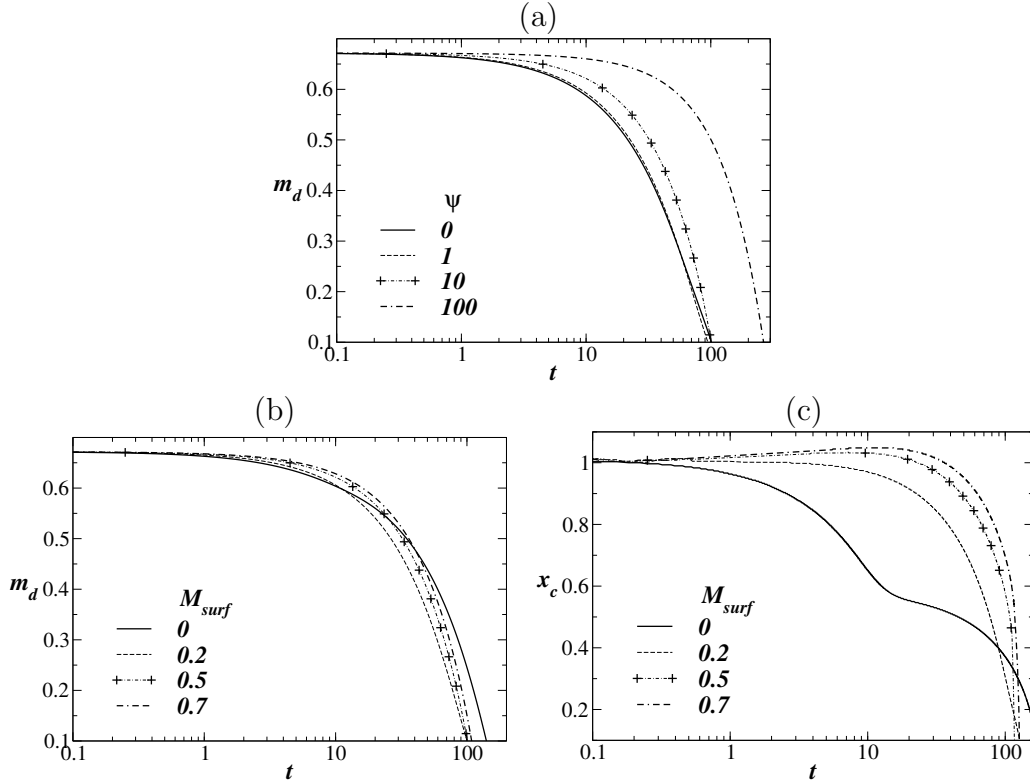


Figure 6: (a) Evolution of the drop mass for different values of ψ and $E = 0.005$. Evolution of (b) mass of the drop, (c) position of the contact line versus time for $\psi = 10$ and different values of M_{surf} . The rest of the parameter values are $E = 0.005$, $M_{par} = 0$, $\chi = 0$ and $\gamma = 0.1$.

deduce that increasing Γ leads to a decrease in the maximal value of J near the contact line. However, this is not reflected in the droplet life-time which decreases with increasing mass of the surfactant as it is shown in Fig. 6(b). To explain this behaviour, it is necessary to investigate the effect of ψ on the spatio-temporal development of h which is shown in Fig. 7. For low values of ψ , the evaporative flux is sufficiently strong so as to induce contact line recession during all stages of the evaporation process. With increasing ψ , however, J decreases leading to droplet evaporation accompanied by spreading; the degree of spreading is particularly pronounced for the largest values of ψ investigated, and persists to advanced

stages of the droplet dynamics (see Fig. 6(c)). From Eq. (49), however, we see that the value of J near the apex is inversely proportional to the droplet thickness, h , which may explain the trends shown in Fig. 6(b), since due to the extensive spreading of the droplet it retains a thinner profile for longer times. Regarding the flow field, we find that the formation of a recirculating vortex in the contact line region is delayed whilst its size remains smaller throughout the simulation (see animation for Fig. 7c in the Supporting Information, Movie S3).

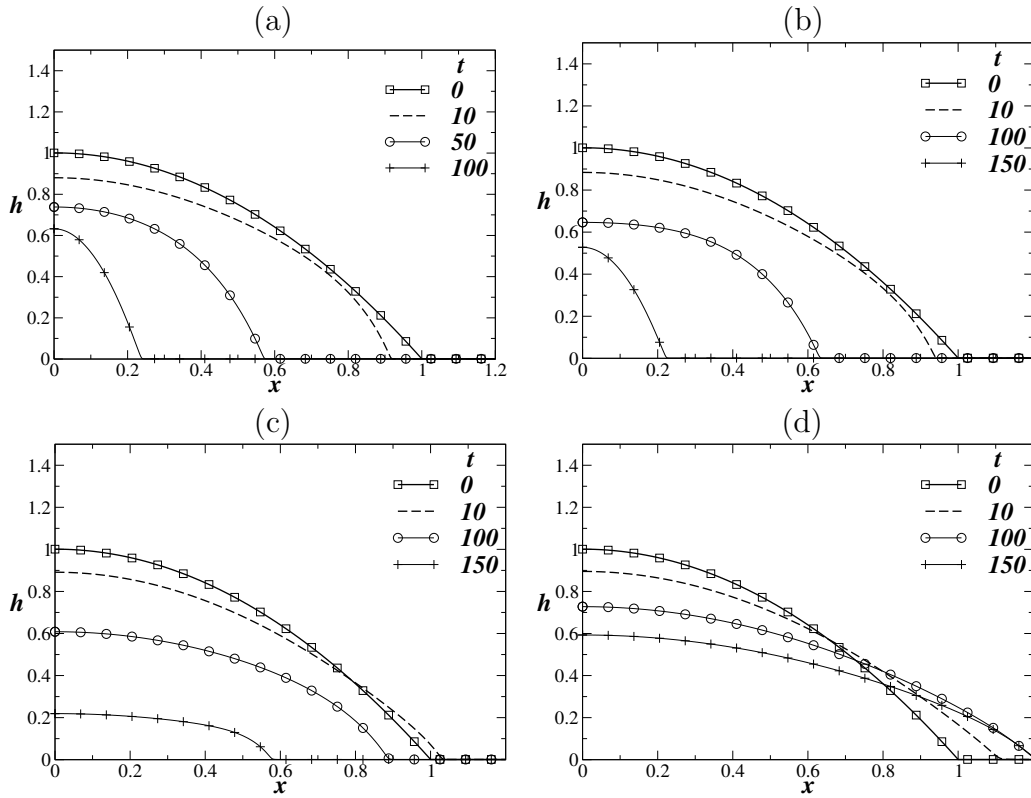


Figure 7: Evolution of the drop height, h , for (a) $\psi = 0$, (b) $\psi = 1$, (c) $\psi = 10$ and (d) $\psi = 100$. The rest of the parameter values are the same as those used to generate Fig. 6(b).

3.2 Surfactant-laden droplets with particles

We continue our study by taking into account the effect of non-interacting, surface-inactive particles in the droplet. Here, we consider finite values of the parameter ψ and therefore take into account the effect of surfactants on the evaporative flux, J . In Fig. 8(a,b), we show

the spatio-temporal variation of the particle concentration in the bulk in the presence and absence of surfactant, respectively. It is seen that at early times c remains approximately constant over a large proportion of the drop before undergoing a rapid increase as the contact line region is approached, which is followed by a decay to zero in the precursor film region. The particle concentration becomes maximum in the contact line region due to the strong

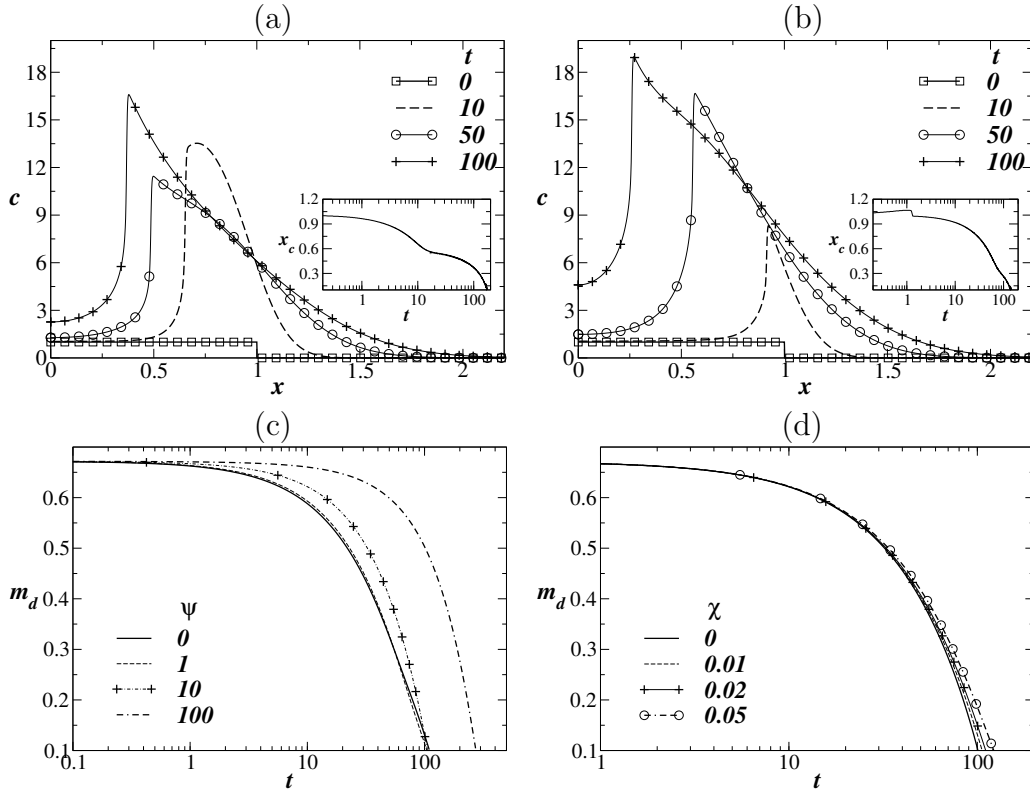


Figure 8: Evolution of particle concentration, c , profile for (a) $M_{surf} = 0$, (b) $M_{surf} = 0.5$ and $\psi = 0$; $\chi = 0.01$. Evolution of droplet mass for different values of (c) ψ for $\chi = 0.01$ and $M_{surf} = 0.5$, and (d) χ for $\psi = 10$ and $M_{surf} = 0.5$. The rest of the parameter values are $E = 0.005$, $M_{par} = 0.666$ and $\gamma = 0.1$. The insets in panels (a) and (b) show the temporal evolution of the contact line position.

capillary flow there; which is responsible for the well known "coffee stain" effect.^{10–12} In the surfactant-free case (see Fig. 8(a)) the rapid retraction of the contact line, due to the effect of thermal Marangoni stresses, at intermediate times leads to a decrease of the maximum particle concentration as some particles are left behind; these particles eventually diffuse away from the droplet. At later stages, though, the contact line decelerates (see insets of Fig. 7(a) showing the temporal variation of x_c) resulting in the increase of particle concentration at the

contact line; the deceleration of the contact line is also enhanced by the increasing viscosity due to the presence of particles (see Eq. (30)). On the other hand, in the surfactant-laden case (see Fig. 8(b)) the slower retraction of the contact line leads to a monotonic increase of the particle concentration in the contact line region. Regarding the droplet life-time, as shown in Fig. 8(c), it does not appear to depend significantly on the presence of particles in the system. On the other hand, varying the value of the parameter ψ we see the same trends in terms of evolution of the droplet mass, m_d as for the particle-free case (see Fig. 8(d)). A typical evolution of the droplet profile along with the velocity field (x -component) and the streamlines are shown in an animation in the Supporting Information (Movie S4) for $E = 0.005$, $M_{surf} = 0.5$, $\psi = 10$, $M_{par} = 0.666$, $\chi = 0.01$ and $\gamma = 0.1$.

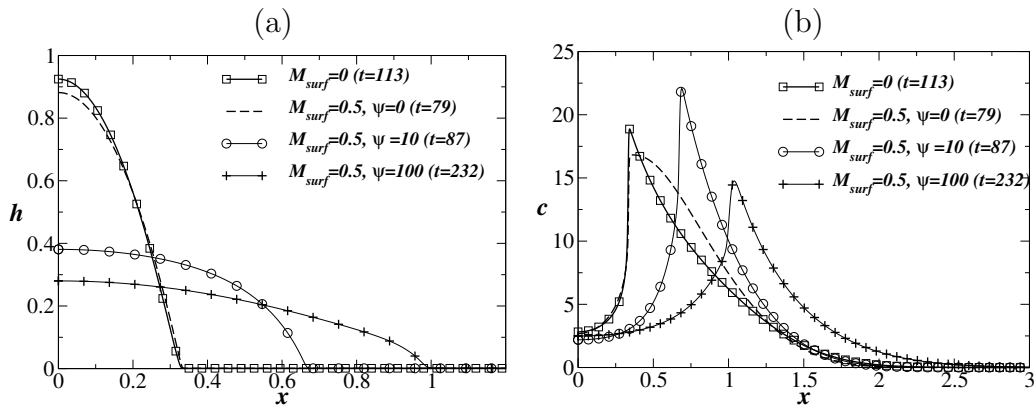


Figure 9: Profiles of drop height, h , and particle concentration, c , at times for which m_d reaches 0.2. The rest of the parameter values are $E = 0.005$, $M_{par} = 0.666$, $\chi = 0.01$ and $\gamma = 0.1$.

The final particle deposition patterns for the various cases under consideration can be evaluated by plotting in Fig. 9(a,b) the droplet shapes and particle concentration profiles, respectively, at times for which the droplet has lost 80% of its initial mass. Evidently, in the case of a particle-laden droplet, its shape at late stages of the evaporation process is significantly affected by the presence of surfactants and the value of the parameter, ψ , as it has already been established for a particle-free drop. Not surprisingly, the difference in the dynamics of evaporation due to the effect of surfactants is also reflected on the particle concentration profile, shown in Fig. 9(b). When we do not take into account the effect of

surfactant on the evaporative flux ($\psi = 0$) we find that the particle concentration profile for the surfactant-free and the surfactant-laden case are quite similar. The plateau that arises in the surfactant-laden case, in contrast to the sharp peak in the surfactant-free case, can be attributed to the somewhat slower retraction of the contact line. For finite values of ψ , though, the deposition patterns are markedly different since high values of ψ appear to promote contact line pinning and thus significantly enhance the "coffee stain" effect.

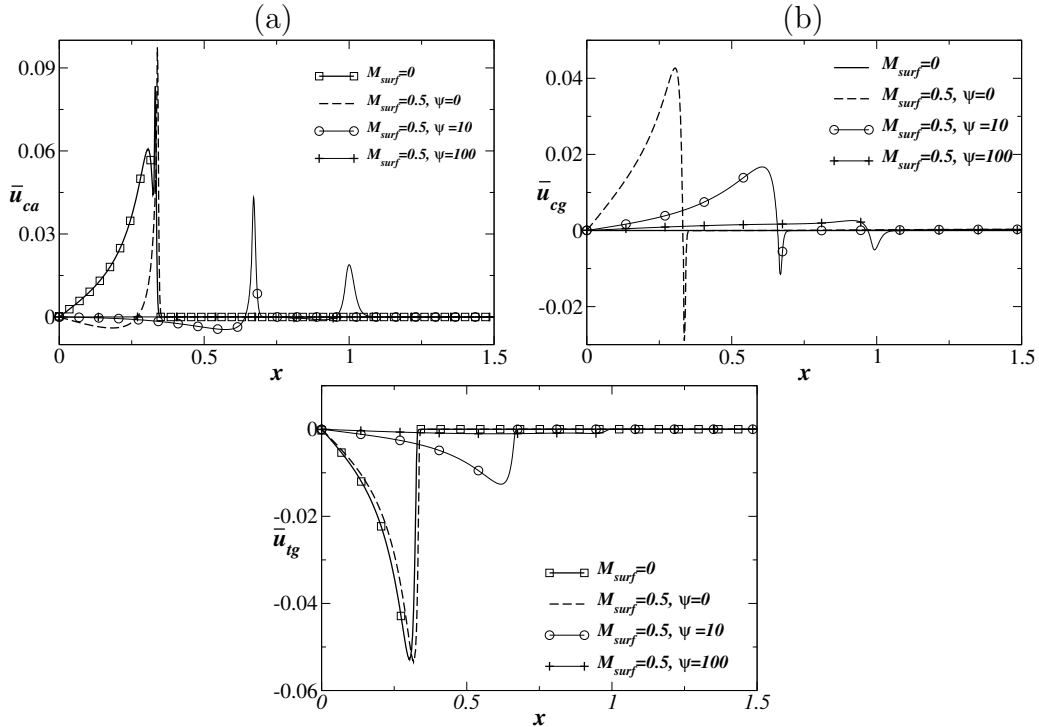


Figure 10: Profiles of \bar{u}_{ca} , \bar{u}_{cg} and \bar{u}_{tg} at times for which m_d reaches 0.2 for different values of M_{surf} and ψ . The rest of the parameter values are $\chi = 0.01$ and $E = 0.005$, $M_{par} = 0.666$ and $\gamma = 0.1$.

In order to identify the physical mechanisms and how they affect the evaporation process of a particle-laden drop we decomposed the average velocity in the bulk into its three main components (see Eq. 40), i.e. flow caused by the effect of capillary pressure, \bar{u}_{ca} , surfactant concentration gradients, \bar{u}_{cg} , and thermal gradients, \bar{u}_{tg} . As shown in Fig. 10, liquid is drawn towards the contact line due to the effect of capillary flow and surfactant concentration gradients, and towards the droplet centre due the effect of thermal gradients. These results are clearly in agreement, with the intuitive ideas and experimental findings presented by Hu

and Larson¹⁵. We also see in Fig. 10 that the capillary flow in the contact line region is enhanced in the case of a surfactant-free droplet or in the presence of surfactants for $\psi = 0$. Finite values of ψ result in the reduction of the effect of capillary flow, mostly due to the fact that the evaporative flux near the contact line decreases significantly due to the presence of surfactant molecules and therefore less liquid has to be drawn in the contact line region from the bulk. The decrease of the capillary flow also leads to less accumulation of surfactant near the contact line which results in smaller concentration gradients and thus reduced effect of the solutal Marangoni stresses. Finally, with increasing value of ψ , the decrease of the evaporative flux also leads to smaller variation of interfacial temperature rendering the effect of thermal Marangoni stresses less pronounced.

4. Conclusions

We have studied the two-dimensional dynamics of a particle-laden volatile droplet on a superheated solid substrate in the presence of surfactants. Lubrication theory and rapid vertical diffusion of the surfactant and particles in the bulk are used in conjunction with asymptotic reduction to simplify the equations of heat, momentum, and mass conservation, and derive a coupled system of evolution equations for the interface height, surfactant monomers and bulk particle concentrations. The model accounts for the effect of solutal and thermal Marangoni stresses, interfacial and bulk diffusion of surfactant monomers and particles, respectively, as well as the effect of a varying viscosity depending on the local particle concentration. Crucially, our model also takes into account that surfactants may inhibit the evaporation rate, by reducing the effective area along the liquid-air interface through which evaporation takes place.

We have used a finite-element formulation and an implicit Euler method in time to solve the system of evolution equations. A parametric study was carried out in order to investigate how the presence of surfactants affects the evaporation process as well as the flow dynamics with and without the presence of particles in the bulk. It is shown that the flow inside

the evaporating droplet is driven by three different mechanisms, i.e. the effect of capillary pressure, solutal and thermal Marangoni stresses, which also play a key role in the final particle deposition pattern. Moreover, the effect of surfactant monomers on the evaporative flux, through the reduction of the effective interfacial area through which evaporation is possible, affects significantly the action of these mechanisms especially near the contact line region. Our simulations indicate that when the effect of surfactant on the evaporative flux is negligible, surfactant-laden, **particle-free** droplets evaporate more rapidly than their surfactant-free counterparts due to suppression of the thermal Marangoni stresses-induced motion by surfactant-driven Marangoni flow. Nevertheless, when the effect of surfactant on the evaporative flux is appreciable, the evaporation process **is retarded** leading to an increase of the droplet life-time. We also show that for particle-laden droplets, the particle deposition patterns are influenced strongly by the direct effect of surfactant on the evaporative flux; in certain cases, the "coffee stain" effect is enhanced significantly.

Acknowledgement

OKM acknowledges the support of the Engineering and Physical Sciences Research Council, UK, through grant numbers EP/K003976 and EP/L020564.

References

- (1) Byun, M.; Laskowski, R. L.; He, M.; Qiu, F.; Jeffries-EL, M.; Lin, Z. Controlled Evaporative Self-Assembly of Hierarchically Structured Regioregular Conjugated Polymers. *Soft Matter* **2009**, *5*, 1583–1586.
- (2) Chen, G.; J. Mohamed, G. Complex Protein Patterns Formation via Salt-Induced Self-Assembly and Droplet Evaporation. *Eur. Phys. J. E* **2010**, *33*, 19–26.
- (3) Han, W.; Lin, Z. Learning from "Coffee Rings": Ordered Structures Enabled by Controlled Evaporative Self-Assembly. *Angew. Chem. Int. Ed.* **2012**, *51*, 1534–1546.

- (4) Sun, Y.; Xiao, G.; Lin, Y.; Su, Z.; Wang, Q. Self-Assembly of Large-Scale P3HT Patterns by Confined Evaporation in the Capillary Tube. *RSC Adv.* **2015**, *5*, 20491–20497.
- (5) Blossey, R.; Bosio, A. Contact Line Deposits on cDNA Microarrays: A "Twin-Spot Effect". *Langmuir* **2002**, *18*, 2952–2954.
- (6) Heim, T.; Preuss, S.; Gerstmayer, B.; Bosio, A.; Blossey, R. Deposition from a Drop: Morphologies of Unspecifically Bound DNA. *J. Phys. Condens. Matter* **2005**, *17*, S703–S716.
- (7) Sefiane, K. Patterns from Drying Drops. *Adv. Colloid Interface Sci.* **2014**, *206*, 372–381.
- (8) Yildirim Erbil, H. Control of Stain Geometry by Drop Evaporation of Surfactant Containing Dispersions. *Adv. Colloid Interface Sci.* **2015**, *222*, 275–290.
- (9) Larson, R. G. Transport and Deposition Patterns in Drying Sessile Droplets. *AIChE J.* **2014**, *60*, 1538–1571.
- (10) Deegan, R. D.; Bakajin, O.; Dupont, T. F.; Huber, G.; Nagel, S. R.; Witten, T. A. Capillary Flow as the Cause of Ring Stains from Dried Liquid Drops. *Nature* **1997**, *389*, 827–829.
- (11) Deegan, R. D.; Bakajin, O.; Dupont, T. F.; Huber, G.; Nagel, S. R.; Witten, T. A. Contact Line Deposits in an Evaporating Drop. *Phys. Rev. E* **2000**, *62*, 756–765.
- (12) Deegan, R. D. Pattern Formation in Drying Drops. *Phys. Rev. E* **2000**, *61*, 475–485.
- (13) Hu, H.; Larson, R. G. Analysis of the Effects of Marangoni Stresses on the Microflow in an Evaporating Sessile Droplet. *Langmuir* **2005**, *21*, 3972–3980.
- (14) Hu, H.; Larson, R. G. Analysis of the Microfluid Flow in an Evaporating Sessile Droplet. *Langmuir* **2005**, *21*, 3963–3971.

- (15) Hu, H.; Larson, R. G. Marangoni Effect Reverses Coffee-Ring Depositions. *J. Phys. Chem. B* **2006**, *110*, 7090–7094.
- (16) Eral, H. B.; Augustine, D. M.; Duits, M. H. G.; Mugele, F. Suppressing the Coffee Stain Effect: How to Control Colloidal Self-Assembly in Evaporating Drops Using Electrowetting. *Soft Matter* **2011**, *7*, 4954–4958.
- (17) Mampallil, D.; Eral, H. B.; van den Ende, D.; Mugele, F. Control of Evaporating Complex Fluids through Electrowetting. *Soft Matter* **2012**, *8*, 10614–10617.
- (18) Orejon, D.; Sefiane, K.; Shanahan, M. E. Evaporation of Nanofluid Droplets with Applied DC Potential. *J. Colloid Interface Sci.* **2013**, *407*, 29–38.
- (19) Wray, A. W.; Papageorgiou, D. T.; Craster, R. V.; Sefiane, K.; Matar, O. K. Electrostatic Suppression of the "Coffee Stain Effect". *Langmuir* **2014**, *30*, 5849–5858.
- (20) Ristenpart, W. D.; Kim, P. G.; Domingues, C.; Wan, J.; Stone, H. A. Influence of Substrate Conductivity on Circulation Reversal in Evaporating Drops. *Phys. Rev. Lett.* **2007**, *99*, 234502.
- (21) Truskett, V. N.; Stebe, K. J. Influence of Surfactants on an Evaporating Drop: Fluorescence Images and Particle Deposition Patterns. *Langmuir* **2003**, *19*, 8271–8279.
- (22) Still, T.; Yunker, P. J.; Yodh, A. G. Surfactant-Induced Marangoni Eddies Alter the Coffee-Rings of Evaporating Colloidal Drops. *Langmuir* **2012**, *28*, 4984–4988.
- (23) Semenov, S.; Trybala, A.; Agogo, H.; Kovalchuk, N.; Ortega, F.; Rubio, R. G.; Starov, V. M.; Velarde, M. G. Evaporation of Droplets of Surfactant Solutions. *Langmuir* **2013**, *29*, 10028–10036.
- (24) Sempels, W.; De Dier, R.; Mizuno, H.; Hofkens, J.; Vermant, J. Auto-Production of Biosurfactants Reverses the Coffee Ring Effect in a Bacterial System. *Nat. Commun.* **2013**, *4*, 1757.

- (25) Crivoi, A.; Duan, F. Amplifying and Attenuating the Coffee-Ring Effect in Drying Sessile Nanofluid Droplets. *Phys. Rev. E* **2013**, *87*, 042303.
- (26) Crivoi, A.; Duan, F. Effect of Surfactant on the Drying Patterns of Graphite Nanofluid Droplets. *J. Phys. Chem. B* **2013**, *117*, 5932–5938.
- (27) Marin, A.; Liepelt, R.; Rossi, M.; Kähler, C. J. Surfactant-Driven Flow Transitions in Evaporating Droplets. *Soft Matter* **2016**, *12*, 1593–1600.
- (28) Morales, V. L.; Parlange, J.-Y.; Wu, M.; Pérez-Reche, F. J.; Zhang, W.; Sang, W.; Steenhuis, T. S. Surfactant-Mediated Control of Colloid Pattern Assembly and Attachment Strength in Evaporating Droplets. *Langmuir* **2013**, *29*, 1831–1840.
- (29) Anyfantakis, M.; Geng, Z.; Morel, M.; Rudiuk, S.; Baigl, D. Modulation of the Coffee-Ring Effect in Particle/Surfactant Mixtures: The Importance of Particle-Interface Interactions. *Langmuir* **2015**, *31*, 4113–4120.
- (30) Bhardwaj, R.; Fang, X.; Somasundaran, P.; Attinger, D. Self-Assembly of Colloidal Particles from Evaporating Droplets: Role of DLVO Interactions and Proposition of a Phase Diagram. *Langmuir* **2010**, *26*, 7833–7842.
- (31) De Dier, R.; Sempels, W.; Hofkens, J.; Vermant, J. Thermocapillary Fingering in Surfactant-Laden Water Droplets. *Langmuir* **2014**, *30*, 13338–13344.
- (32) Barnes, G. T. The Effects of Monolayers on the Evaporation of Liquids. *Adv. Colloid Interface Sci.* **1986**, *25*, 89–200.
- (33) Lunkenheimer, K.; Zembala, M. Attempts to Study a Water Evaporation Retardation by Soluble Surfactants. *J. Colloid Interface Sci.* **1997**, *188*, 363–371.
- (34) Barnes, G. The Potential for Monolayers to Reduce the Evaporation of Water from Large Water Storages. *Agric. Water Manage.* **2008**, *95*, 339–353.

- (35) Davies, J. F.; Miles, R. E. H.; Haddrell, A. E.; Reid, J. P. Influence of Organic Films on the Evaporation and Condensation of Water in Aerosol. *Proc. Natl. Acad. Sci.* **2013**, *110*, 8807–8812.
- (36) Hamzah, M. H.; Zain, S. M.; Khan, R. A.; Khalid, K. Study the Effect of Imposing Surfactants toward the Evaporation of Low Molecular Weight Alcohol. *Int. J. Env. Sci. Dev.* **2013**, 403–407.
- (37) Mikishev, A. B.; Nepomnyashchy, A. A. Instabilities in Evaporating Liquid Layer with Insoluble Surfactant. *Phys. Fluids* **2013**, *25*, 054109.
- (38) Clay, M. A.; Miksis, M. J. Effects of Surfactant on Droplet Spreading. *Phys. Fluids* **2004**, *16*, 3070.
- (39) Chan, K. Y.; Borhan, A. Surfactant-Assisted Spreading of a Liquid Drop on a Smooth Solid Surface. *J. Colloid Interface Sci.* **2005**, *287*, 233–248.
- (40) Beacham, D. R.; Matar, O. K.; Craster, R. V. Surfactant-Enhanced Rapid Spreading of Drops on Solid Surfaces. *Langmuir* **2009**, *25*, 14174–14181.
- (41) Karapetsas, G.; Craster, R. V.; Matar, O. K. On Surfactant-Enhanced Spreading and Superspreading of Liquid Drops on Solid Surfaces. *J. Fluid Mech.* **2011**, *670*, 5–37.
- (42) Craster, R. V.; Matar, O. K.; Sefiane, K. Pinning, Retraction, and Terracing of Evaporating Droplets Containing Nanoparticles. *Langmuir* **2009**, *25*, 3601–3609.
- (43) Kaplan, C. N.; Mahadevan, L. Evaporation-Driven Ring and Film Deposition From Colloidal Droplets. *J. Fluid Mech.* **2015**, *781*.
- (44) Burelbach, J. P.; Bankoff, S. G.; Davis, S. H. Nonlinear Stability of Evaporating/Condensing Liquid Films. *J. Fluid Mech.* **1988**, *195*, 463–494.
- (45) Ajaev, V. S.; Homsy, G. M. Steady Vapor Bubbles in Rectangular Microchannels. *J. Colloid Interface Sci.* **2001**, *240*, 259–271.

- (46) Ajaev, V. S. Spreading of Thin Volatile Liquid Droplets on Uniformly Heated Surfaces. *J. Fluid Mech.* **2005**, *528*, 279–296.
- (47) Karapetsas, G.; Matar, O. K.; Valluri, P.; Sefiane, K. Convective Rolls and Hydrothermal Waves in Evaporating Sessile Drops. *Langmuir* **2012**, *28*, 11433–11439.
- (48) Sultan, E.; Boudaoud, A.; Amar, M. B. Evaporation of a Thin Film: Diffusion of the Vapour and Marangoni Instabilities. *J. Fluid Mech.* **2005**, *543*, 183.
- (49) Warner, M.; Craster, R.; Matar, O. Surface Patterning via Evaporation of Ultrathin Films Containing Nanoparticles. *J. Colloid Interface Sci.* **2003**, *267*, 92–110.
- (50) Bligh, P. H.; Haywood, R. Latent Heat-Its Meaning and Measurement. *Eur. J. Phys.* **1986**, *7*, 245–251.
- (51) Krieger, I. M. A Mechanism for Non-Newtonian Flow in Suspensions of Rigid Spheres. *J. Rheol.* **1959**, *3*, 137–152.
- (52) Barnes, H. A. The Yield Stress - A Review or "Πάντα Ρεῖ" - Everything Flows? *J. Non-Newt. Fluid Mech.* **1999**, *81*, 133–178.
- (53) Kaplan, C. N.; Wu, N.; Mandre, S.; Aizenberg, J.; Mahadevan, L. Dynamics of evaporative colloidal patterning. *Phys. Fluids* **2015**, *27*, 092105.
- (54) Wong, H.; Rumschitzki, D.; Maldarelli, C. On the Surfactant Mass Balance at a Deforming Fluid Interface. *Phys. Fluids* **1996**, *8*, 3203–3204.
- (55) Pereira, A.; Kalliadasis, S. On the Transport Equation for an Interfacial Quantity. *Eur. Phys. J. Appl. Phys.* **2008**, *44*, 211–214.
- (56) Sheludko, A. Thin Liquid Films. *Adv. Colloid Interface Sci.* **1967**, *1*, 391–464.
- (57) Gaver, D. P.; Grotberg, J. B. The Dynamics of a Localized Surfactant on a Thin Film. *J. Fluid Mech.* **1990**, *213*, 127–148.

- (58) Moosman, S.; Homsy, G. M. Evaporating Menisci of Wetting Fluids. *J. Colloid Interface Sci.* **1980**, *73*, 212–223.
- (59) Karapetsas, G.; Craster, R. V.; Matar, O. K. Surfactant-Driven Dynamics of Liquid Lenses. *Phys. Fluids* **2011**, *23*, 122106.
- (60) Jensen, O. E.; Grotberg, J. B. The Spreading of Heat or Soluble Surfactant Along a Thin Liquid Film. *Phys. Fluids A* **1993**, *5*, 58–68.
- (61) Bhardwaj, R.; Fang, X.; Attinger, D. Pattern Formation During the Evaporation of a Colloidal Nanoliter Drop: a Numerical and Experimental Study. *New Journal of Physics* **2009**, *11*, 075020.